



PCCP

**Liquid-phase decomposition mechanism for
bis(triaminoguanidinium) azotetrazolate (TAGzT)**

Journal:	<i>Physical Chemistry Chemical Physics</i>
Manuscript ID	CP-ART-01-2020-000183.R2
Article Type:	Paper
Date Submitted by the Author:	11-Mar-2020
Complete List of Authors:	Kumbhakarna, Neeraj; IIT Bombay, Mechanical Engineering Khichar, Mayank; Pennsylvania State University Shah, Kaushal; Intralox LLC Chowdhury, Arindrajit; IIT Bombay, Mechanical Engineering Patidar, Lalit; Pennsylvania State University Thynell, Stefan; Pennsylvania State University

SCHOLARONE™
Manuscripts

Liquid-phase decomposition mechanism for bis(triaminoguanidinium) azotetrazolate (TAGzT)

Neeraj R. Kumbhakarna,^a Mayank Khichar,^b Kaushal J. Shah,^c Arindrajit Chowdhury,^a Lalit Patidar,^b and Stefan T. Thynell^{*b}

Received 00th January 20xx,
Accepted 00th January 20xx

DOI: 10.1039/x0xx00000x

This work provides new insights for the liquid-phase decomposition of bis(triaminoguanidinium) azotetrazolate (TAGzT). The liquid-phase decomposition process was investigated using a combined experimental and computational approach. Sub-milligram samples of TAGzT were heated at rates of about 2000 K/s to a set temperature (230 to 260 °C) where liquid-phase decomposition occurred under isothermal conditions. Fourier transform infrared (FTIR) spectroscopy and time-of-flight mass spectrometry (ToFMS) were used to acquire transmittance spectra and mass spectra of the evolved gas-phase species from the rapid thermolysis, respectively. FTIR spectroscopy was also used to acquire the transmittance spectra of the condensate and residue formed from the decomposition. N₂, NH₃, HCN, N₂H₄, triaminoguanidine and 3-azido-1,2,4-triazol-4-ide anion were identified as products of liquid-phase decomposition. Quantum chemical calculations were used for confirming the identity of the species observed in experiments and for identifying elementary chemical reactions that formed these species. Based on the calculated free energy barriers of these elementary reactions, important reaction pathways were identified for the formation of each of the product species.

Introduction

High-nitrogen energetic materials derive their energy from high positive heats of formation and produce less smoke compared to traditional propellants at lower adiabatic flame temperatures during combustion.¹⁻⁴ A recently synthesized nitrogen-rich material, TAGzT, has attracted attention due to its potential to act as a gun-propellant,⁵ gas-generator for airbags,² and a burn-rate enhancer for traditional energetic materials such as RDX⁶⁻⁹. The current knowledge available for decomposition of TAGzT is not enough to predict the combustion behaviour of its composite propellants. To understand mixture compatibility, thermal stability, and combustion behaviour, thorough knowledge of thermolysis of each of the individual components in the propellant mixture is required. Numerous studies describe the thermal decomposition and combustion behaviour of conventional propellants such as RDX and HMX.¹⁰⁻¹⁴ However, the thermal decomposition behaviour of azotetrazolates has been the subject of relatively fewer studies. Hence, this work focuses on understanding the condensed-phase decomposition process of TAGzT. A review of available decomposition studies on TAGzT is presented next.

TAGzT is a bright yellow crystalline solid with a distinct melting point of 195 °C and 1.6 g/cm³ density. The molecular structure of TAGzT is shown in Fig. 1. Bracuti and Marchak performed X-ray diffraction studies to determine the crystal and molecular structure of TAGzT.¹⁵ Behler et al. studied structural variations due to external pressure using Raman spectroscopy.¹⁶ Hammerl et al. determined various explosive properties using vibrational and NMR spectroscopy, elemental analysis, and safety tests.¹⁷ Burning rate experiments, T-jump/FTIR spectroscopy measurements, and laser-ignition studies were performed by Tappan et al.¹⁸ It was found that TAGzT has extremely high low-pressure burn rates compared to conventional explosives, such as RDX and HMX. The authors concluded that the ignition and decomposition behaviour of TAGzT was controlled by condensed-phase reactions. Thermogravimetric analysis (TGA), differential thermal analysis (DTA), FTIR spectrometry, and mass spectrometry experiments were performed by Damse et al.¹⁹ They stated that rapid initial exothermic decomposition of the nitrogen-rich TAGzT is responsible for its high burn rate. More recently, the decomposition of TAGzT was studied by Hayden.²⁰ She investigated the underlying chemical and physical processes

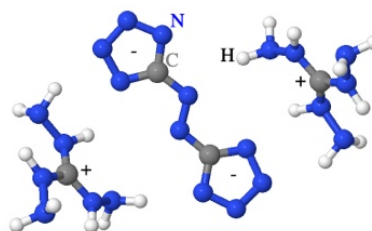


Fig. 1 Molecular structure of bis(triaminoguanidinium) azotetrazolate.

^a Department of Mechanical Engineering, IIT Bombay, Mumbai, Maharashtra 400076, India.

^b Department of Mechanical Engineering, The Pennsylvania State University, University Park, PA, 16802, USA.

^c Intralox, Hanover, MD 21076, USA.

* Corresponding author e-mail: thynell@psu.edu (S.T. Thynell)

† Electronic supplementary information (ESI) available: Decomposition reactions with activation barriers and structures of intermediate species and transition states provided.

that control the thermal decomposition behaviour of TAGzT alone and in the presence of RDX. The methods used were simultaneous thermogravimetric modulated beam mass spectrometry and Fourier-transform ion cyclotron resonance mass spectrometry involving slow heating rates (~ 10 °C/min).

The literature survey on TAGzT decomposition presented here indicates that most of these studies used experimental techniques to identify the major reaction pathways. However, in our experience, identification of the major reaction pathways using experimental data alone is quite challenging. Thus, it is essential to explore other approaches to interpret experimental information. Here, we adopt recently developed methods based on the use of quantum chemical calculations. As described in several works, the use of quantum chemical calculations has been quite informative.^{21–24} The results, which include transition states and thermodynamic properties, produced by these techniques can be used to formulate comprehensive reaction mechanisms.^{25, 26} In the present work, FTIR and ToFMS experiments have been performed on TAGzT to analyse its decomposition in the liquid phase, and formation of the observed products has been explained by formulating elementary chemical reactions based on quantum chemical calculations.

Experimental setup and procedure

TAGzT was obtained from the Los Alamos National Laboratory and used without further purification.

Fourier Transform Infrared (FTIR) Spectroscopy

To study the thermal decomposition of TAGzT in the liquid phase, we used the confined rapid thermolysis (CRT) technique^{27, 28} coupled with FTIR spectroscopy. This technique has also been used successfully in previous studies on various energetic materials.^{29, 30} CRT is suitable for the current study because it favours sample decomposition in the liquid phase; evolved species from the sample are quenched by the relatively cooler inert environment. In CRT experiments, a sub-milligram sample is rapidly heated (2000 K/s) to a set temperature where decomposition occurs under near isothermal conditions. The evolved decomposition products are characterised using FTIR spectroscopy. The identity and evolution rates of the decomposition products help identify the pathways for their production.

In our experiments, about 0.5 to 1 mg of TAGzT samples were subjected to thermolysis temperatures ranging from 230 to 260 °C. The spectra for the evolved gaseous products were obtained in near real-time with a spectral resolution of 2 cm^{-1} and a temporal resolution of 50 milliseconds. The measurement time was kept 10 seconds which is sufficient to capture the initial decomposition process of TAGzT in the selected temperature range.

Attempts were also made to identify the heavier liquid-phase decomposition products which condense out quickly from the gas-phase and are difficult to detect in a typical CRT/FTIR experiments. In these experiments, decomposition products were allowed to condense on a glass slide. The

condensate on the slide was then mixed with 150 mg of potassium bromide (KBr) and pressed into a pellet. The pressed pellet was then placed inside a specially designed fixture and its IR spectrum was acquired. The fixture is designed such that it can hold both the sample and pure KBr pellets, and either of them can be aligned in the path of the infrared beam by operating a slider. Effects of direct KBr adsorption on the sample spectrum were removed by using an IR spectrum of pure KBr pellet as background.

Some of the experiments were also performed with an objective to identify the initial liquid-phase decomposition products. This information is crucial to identify the specific bonds which break first, and hence the initiation reactions. In these experiments, TAGzT samples were heated for a period of 4, 8, and 12 seconds at a temperature in 230–250 °C range. The residue left behind on the sample holder was pressed into a KBr pellet and analysed in a similar way as described before.

Time of Flight Mass Spectrometry (ToFMS)

To confirm the identity of liquid-phase decomposition products of TAGzT identified from the coupled CRT-FTIR experiments and to identify IR-inactive decomposition products, we coupled our CRT setup with a time-of-flight (ToF) mass spectrometer. In this system, molecular beam sampling was done by directing the evolved gases towards a 100 μm orifice, which separates the first stage of the vacuum system of the ToF mass spectrometer from the CRT sample chamber. The ToFMS system was equipped with a 1 m flight tube and a 44 mm microchannel plate detector. Additional ToFMS setup and procedural details are described by Chowdhury and Thynell.²⁹ Similar to the coupled CRT/FTIR experiments, about 0.5 to 1 mg of TAGzT samples were subjected to pre-set temperatures (230 to 260 °C). The ToFMS system was also set to collect the data for 10 seconds.

Molecular modelling

Quantum chemical calculations supplement the data obtained from CRT/FTIR and CRT/ToFMS experiments. The Gaussian 09 software package was utilized to this end.³¹ Molecular structures of species involved in the decomposition of TAGzT were identified from ground-state and transition-state optimization calculations. The search for transition states was in most cases performed by using the B3LYP/6-31G(d) level of theory.^{32, 33} The optimized structures served as an initial guess to the B3LYP/6-311++G(d,p) level of theory which employs a triple split-valence basis set with additional polarized functions and accounts for the significant charge delocalization in the ions present.³⁴ All the molecular structures were also optimized and thermodynamic parameters computed using the CBS-QB3 compound method developed by Montgomery et al.³⁵ This method was chosen because it gives a good balance between accuracy and computational effort. In most cases, values obtained from CBS-QB3 method were used, in which the B3LYP method is used in the frequency calculation. For cases in which large discrepancies were observed in the enthalpy and free energy values of the structures between B3LYP and CBS-QB3,

the MP2 perturbation theory³⁶ along with 6-311++G(d,p) basis set and the compound G4(MP2) theory³⁷ were additionally used. Vibrational frequency calculations were performed on all the optimized structures thus obtained to ensure that local energy minima (in case of reactants and products) and saddle points (in case of transition states) were achieved. Transition-state optimizations corresponding to all the proposed reactions were also subjected to IRC (intrinsic reaction coordinate) calculations^{38, 39} using B3LYP/6-31G(d) to ascertain that the transition state indeed connected the reactants to the products. Because our focus is on chemical reactions in the liquid phase, the polarizable continuum model (PCM) using the integral equation formalism variant (IEFPCM)^{40, 41} was used to reflect the assumption that the liquid-phase reactions can be treated as occurring in a solution phase. This model accounts for the continuum solvation effects. The UFF (universal force field) radius, which is the default option in Gaussian 09, was used to build the cavity in PCM. Typical polar solvent, Acetonitrile (CH₃CN) with a dielectric constant of 35.688, was specified as the solvent in all the optimization, frequency and IRC calculations to represent the solution-phase medium. Ramos et al. reported that the solvent can significantly affect the rates of some reactions.⁴² Hence, we used other solvents to ascertain the effect of solvent type on the computed thermodynamic properties. By using acetone, methanol, nitromethane, and water as the solvent, the differences in heats of reaction and

activation enthalpies in most cases did not exceed by more than 0.25 kcal/mol compared to the results obtained by using acetonitrile. This finding is similar to the conclusion reached by other investigators.^{22, 43}

Results and discussion

Experimental results

To understand the decomposition mechanism of TAGzT using the experimentally obtained IR spectra of its decomposition products, it is important to first identify the different peaks in the IR spectrum of the initial TAGzT sample. To this end, we used predicted IR spectra of the triaminoguanidinium (TAG⁺) cation and the azobistetrazolate (AzT²⁻) dianion along with an experimentally obtained spectrum for triaminoguanidine nitrate (TAGN), shown in Fig. 2. For both TAGzT and TAGN the IR spectra were obtained by pressing the samples in KBr pellets. TAGN was purchased from Sigma Aldrich and used without further purification. The spectra for TAG⁺ and AzT²⁻ were predicted using the Gaussian 09 program package³¹ and CBS-QB3 compound method³⁵ with anharmonic corrections. In the CBS-QB3 compound method, geometry optimization and harmonic frequency calculation step are carried out at B3LYP/6-311G(2d,d,p) level of theory. It is clear that the predicted spectrum of AZT²⁻ is very accurate since all the predicted peaks can be observed in the experimentally obtained spectrum of

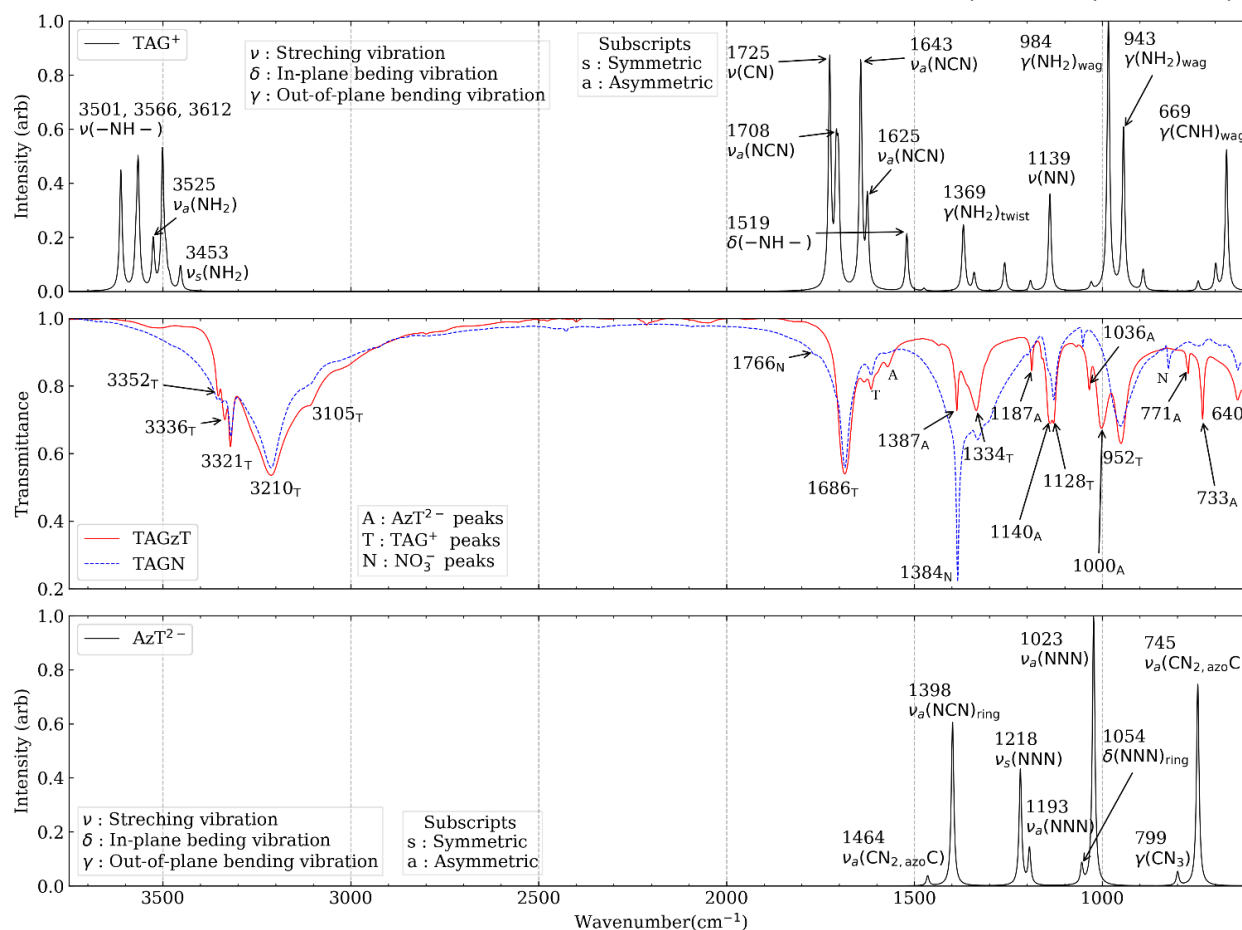


Fig. 2 Comparison of measured spectra for TAGzT and TAGN with the predicted spectra of TAG⁺ and AzT²⁻ in the wavenumber range of 600 to 3750 cm⁻¹.

TAGzT. For TAG⁺, even with the anharmonic corrections, the location of experimentally obtained peaks shift considerably compared to the predicted peaks. This is due to a large number of hydrogen atoms present in TAG⁺ cation, causing significant spectral shifts due to intramolecular and intermolecular hydrogen bonding. To the best of our knowledge, an exact match between experimental and predicted spectra for TAGzT in the liquid phase is not possible using any of the current quantum chemical calculation methods.

With the help of the predicted spectra of TAG⁺ and AzT²⁻ and the experimental spectrum of TAGN, we identified the peaks in the TAGzT spectrum which are due to TAG⁺ and AzT²⁻, shown in Fig. 2. In general, vibrational motions are complex and involve many atoms simultaneously. Here an attempt has been made to account for what appears to be the major atoms involved in the vibrational motion. For TAG⁺ cation, the predicted bands at 943 and 984 cm⁻¹ are due to the wagging motion of NH₂ groups. Predicted bands at 3453 and 3525 cm⁻¹ are due to symmetric and asymmetric vibration of NH₂, respectively. 1369 cm⁻¹ band corresponds to the twisting motion of NH₂. Similarly, for AzT²⁻ dianion, the predicted band at 745 and 1464 cm⁻¹ correspond to the symmetric stretching of –CN_{2,azo}C– group. Note that even though the predicted peak locations are not exact, the changes in heights of these peaks during the decomposition process help identify the structure of the intermediate product species. Fig. 2 shows many other peaks with corresponding nature of vibrational motion and involved atoms, and are not discussed here for brevity.

Fig. 3, Fig. 4, and Fig. 5 show the variation of spectral transmittance of the condensed phase with time for the decomposition temperatures of 230, 240 and 250 °C,

respectively. A close inspection reveals significant changes in bands belonging to AzT²⁻. Minor changes are also observed for bands belonging to ν(N–H) vibration of TAG⁺. Some of the results in the range from 600 to 1100 cm⁻¹ may be affected by noise referred to as channel spectra. This type of noise may occur as a result of internal reflection within the sample. Nonetheless, at the decomposition temperature of 230 °C, the gradual disappearance of the AzT²⁻ bands are very clear, whereas the bands associated with TAG⁺ change quite slowly. The results for this temperature may even suggest that bands associated with vibrations of the carbon atom within AzT²⁻ disappear slower than the other bands, which may suggest that N₂ release from the ring occurs first. Furthermore, a few new bands appear and a very slight shift in a few bands from AzT²⁻ is noticed as well. As the temperature is increased from 230 to 250 °C, the disappearance of AzT²⁻ peaks become rapid. In fact, for the decomposition temperature of 250 °C AzT²⁻ completely decomposes within 4 seconds. In contrast to this, AzT²⁻ was observed to survive for up to 12 seconds in the confined rapid thermolysis of guanidinium azotetrazolate (GzT) at a much higher temperature (280 °C).⁴⁴ This shows that the AzT²⁻ structure in bis(guanidinium) azotetrazolate (GzT) is more stable as compared to that in TAGzT.

Reactions among the decomposition products from AzT²⁻ and decomposition of the cation produce many new bands and thus represent new products that remain in the condensed-phase. Regarding the disappearance of two ν(N–H) stretches near 3340 cm⁻¹, it can be caused by either proton transfer or by increased intermolecular or intramolecular hydrogen bonding, or both. Since the TAG⁺ bands in the range 900–1700 cm⁻¹ are not changing significantly at the decomposition temperature of

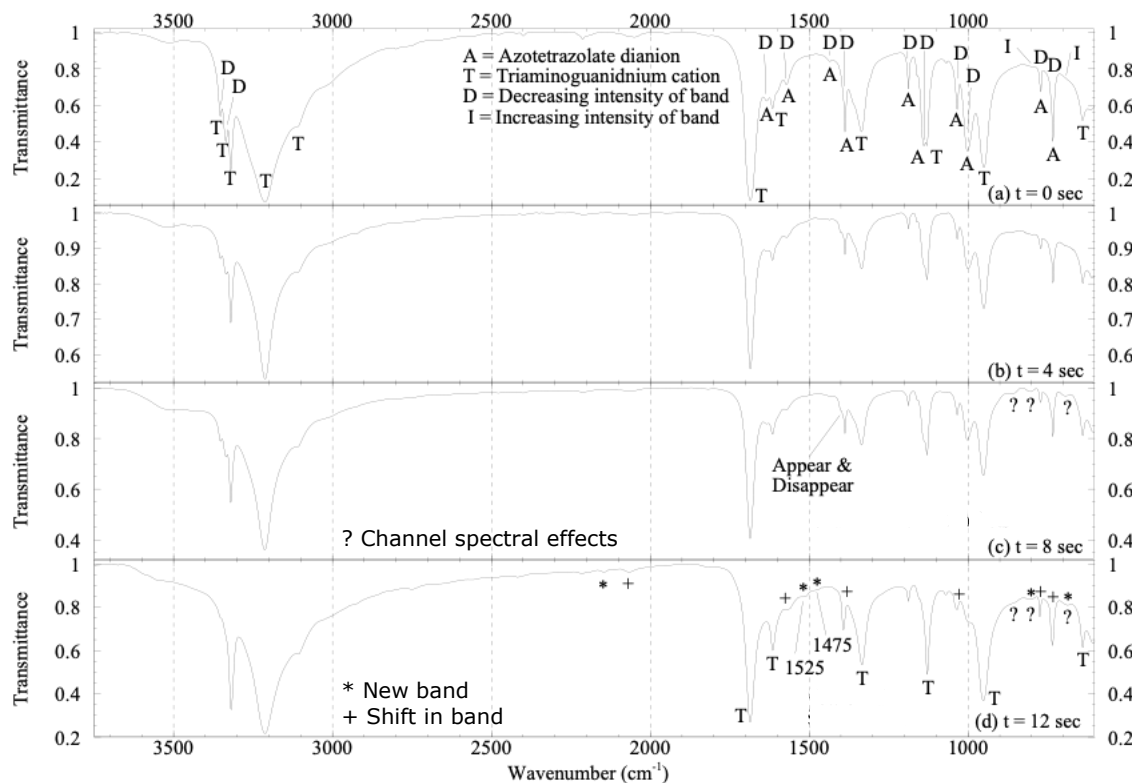


Fig. 3 FTIR spectra of the residue remaining on the foil after thermolysis of TAGzT for a period of 4, 8, and 12 s at 230 °C.

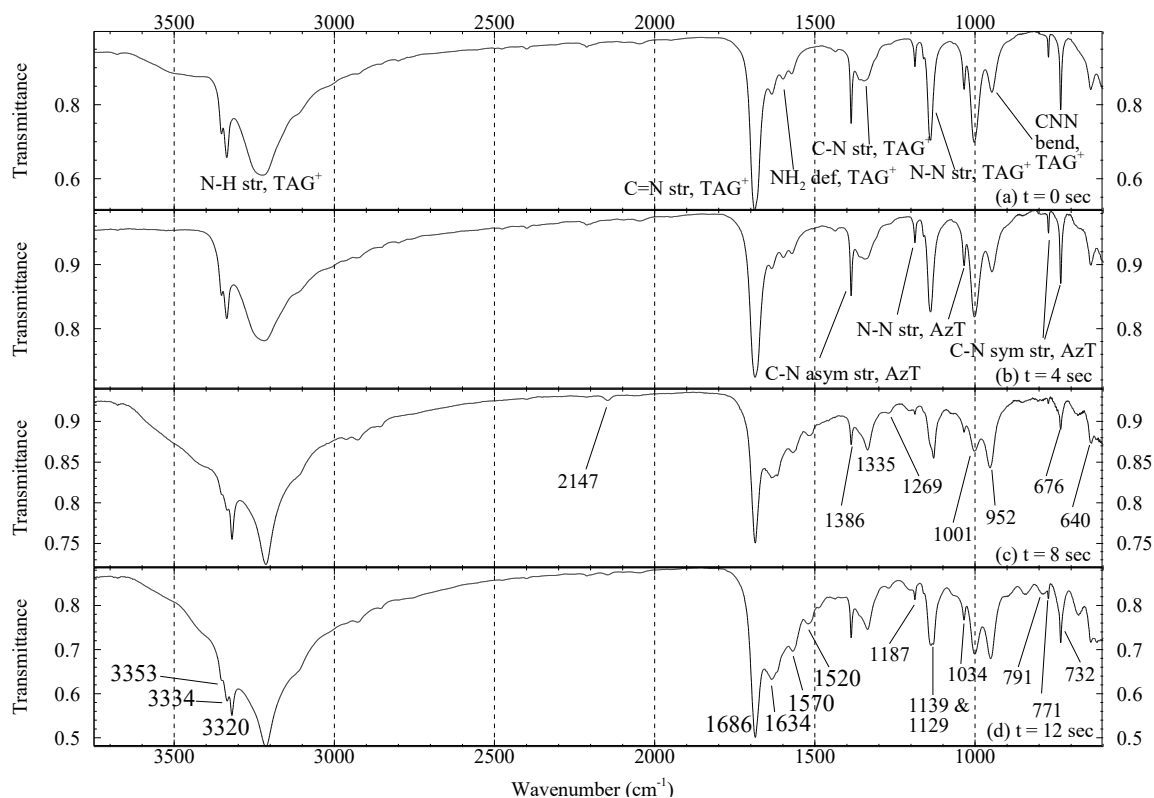


Fig. 4 FTIR spectra of the residue remaining on the foil after thermolysis of TAGzT for a period of 4, 8, and 12 s at 240 °C.

230 °C, it is likely that intermolecular bonding increases due to reduced effects of a steric hindrance as the dianion decomposes. As a result, the sharp band at 3321 cm⁻¹ is then

likely a stretch from the imino hydrogen. The bands attributed to TAG⁺ change otherwise in a very limited fashion at 230 °C, whereas much larger changes are observed at 250 °C. Since the

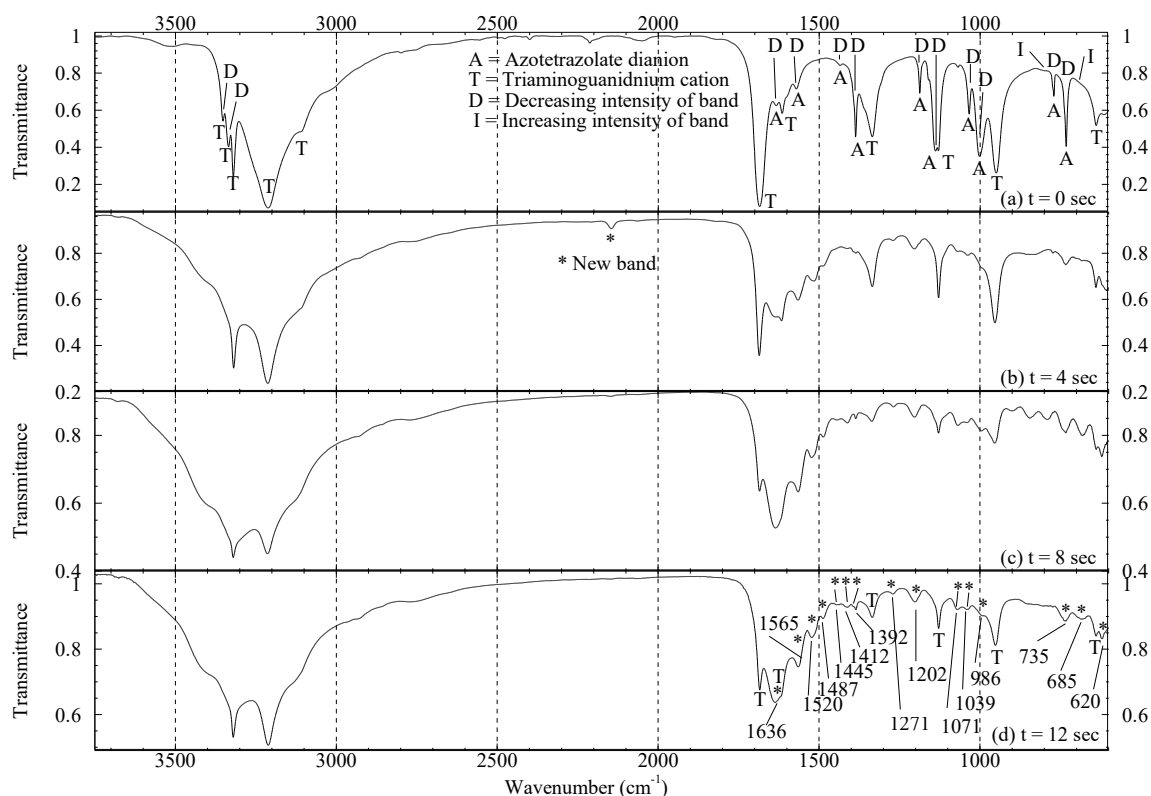


Fig. 5 FTIR spectra of the residue remaining on the foil after thermolysis of TAGzT for a period of 4, 8, and 12 s at 250 °C.

guanidine-based molecules have very large pK_a values, it is highly likely that new anions may be formed and present in the condensed phase.

Fig. 6 shows the spectral transmittance of the condensate collected on a glass slide placed in close vicinity of the opening

Fig. 7 shows the FTIR spectra of gas-phase species evolving into the modulated beam of the FTIR spectrometer from the decomposition of TAGzT at 250 °C. Here, six spectra are averaged near both $t = 2.8$ s and 4.8 s to reduce the effects of random noise. Bands belonging to hydrazine (N_2H_4) overlapped

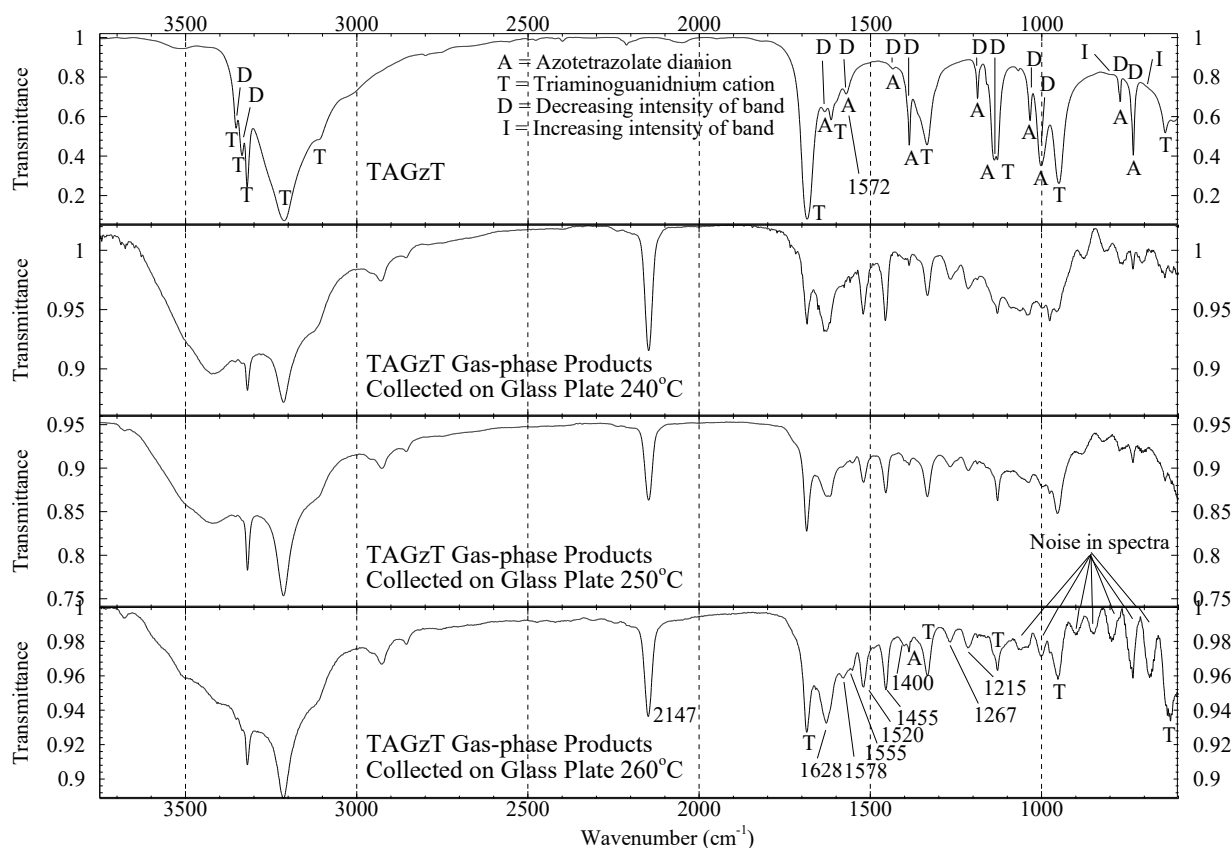


Fig. 6 FTIR spectra of products from thermolysis of TAGzT condensed on a glass slide placed outside the confined thermolysis region over a 20 s time interval at temperatures of 240, 250 and 260 °C.

of the exit hole of the confined region in the thermolysis chamber as described in the experimental setup and procedure section. The high molecular weight species condense on the glass plate, whereas small molecular weight species do not. Thus NH_3 , N_2H_4 , and HCN are absent. It is clear that some triaminoguanidine (TAG) evaporates from the confined region, and it accumulates on the glass plate. Proton transfer also occurs in the condensed phase on the glass plate and many bands match with the previously presented information. However, at the high temperature of 260 °C, much of the collected triaminoguanidine remains neutral, as the amount of proton-donating species collected on the glass plate is significantly reduced, such as HCN . A strong band at 2147 cm^{-1} appears prominently, whereas this band was barely seen in the residue spectra from the condensed phase, refer Fig. 3, Fig. 4, Fig. 5, and Fig. 6. Since this band appears prominently at all temperatures, it is potentially a proton-donating species. When comparing band appearances in Fig. 5 with those of Fig. 6, it is clear that only a few bands are identical. However, the region between 600 and 1100 cm^{-1} is difficult to interpret as noise from channel spectra is significant.

with ammonia which evolves early and gradually. Simultaneous to the evolution of hydrazine, the band at 2147 cm^{-1} is observed. As will be subsequently discussed in the next section, hydrazine is a product of TAG^+ decomposition, and it could be formed via cleavage of weak N–N bonds whereas the band at 2147 cm^{-1} belongs to a ring-opening product of AzT^{2-} . As these products evolve, HCN is also observed, indicating the decomposition of the azotetrazolate ring. The band near 3510 cm^{-1} is strikingly similar in shape and position to a band caused by a stretching vibration from a hydrogen atom attached to a nitrogen atom on a ring as indicated in Fig. 7. Billes et al. provided the vibrational frequencies from both measurements and prediction of 1H-1,2,4-triazole, 1H-tetrazole, and 2H-tetrazole.⁴⁵ Their condensed-phase experimental data reveal the $\nu(N-H)$ stretch position at 3447 cm^{-1} for all three molecules.

In our gas-phase measurements, the $\nu(N-H)$ stretch is located at 3512 cm^{-1} for the 1H-1,2,4-triazole. Thus, there is a difference of about 70 cm^{-1} for this particular band between gas and condensed phases. The $\nu(C-H)$ stretch, however, is at 3119 cm^{-1} for both our gas-phase measurements and the condensed-phase spectra by Billes et al.⁴⁵ In a recent paper on the synthesis of 5-azido-1H-tetrazole⁴⁶, condensed-phase spectra indicate the $\nu(N-$

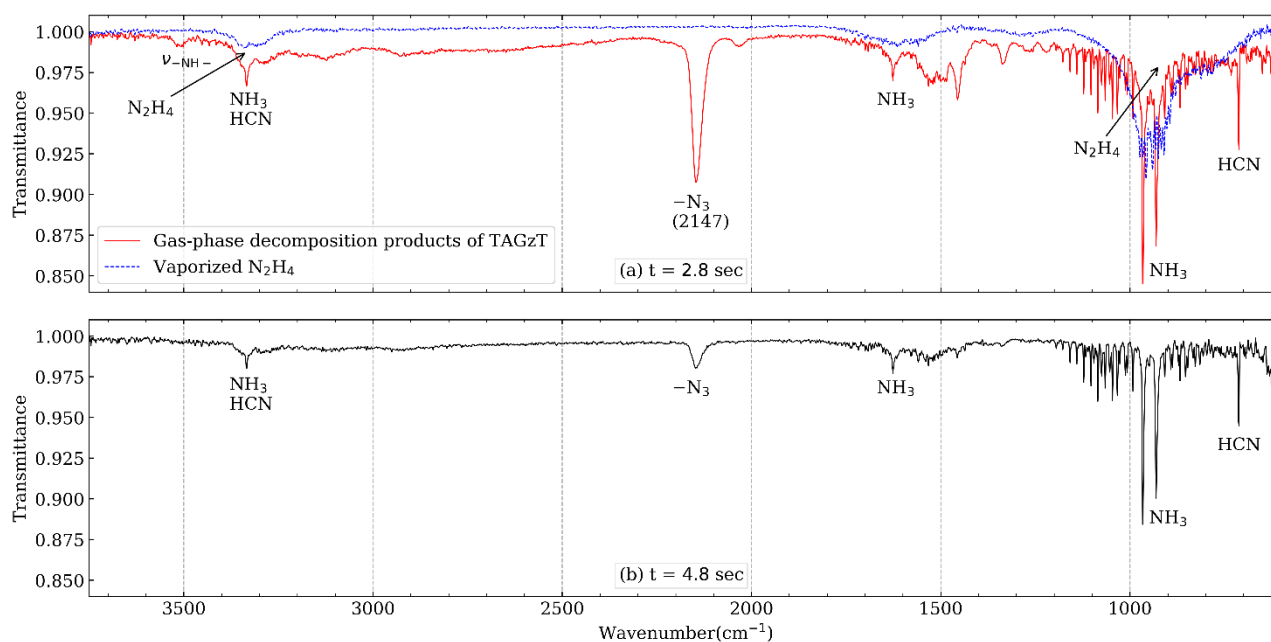


Fig. 7 FTIR spectra showing the gas-phase species evolved during the decomposition of TAGzT at 250 °C and 1 atm N_2 .

H) stretch to be at 3343 cm^{-1} with a weak intensity; even if this spectral location is shifted by 70 cm^{-1} , the band coincides with similar stretches for both hydrazine and ammonia and thus is difficult to distinguish. However, it is likely that the band near 3510 cm^{-1} for our gas-phase measurements arises from a 1H-tetrazole based structure or 1H-triazole itself. As a result of this $\nu(\text{N-H})$, the proton transfer must have occurred at some point during the decomposition of TAGzT. The proton most probably migrates to the AzT^{2-} dianion and attaches itself to either N atom next to the carbon or the adjacent N on the ring.

There are several additional important aspects regarding the gas-phase spectra, and these are described without showing additional figures. First, one notices that the $\nu(\text{N-H})$ band appears strong and subsequently decreases in intensity as the number of acquired spectra increases. Second, if one closely monitors the peak position of the very strong band at 2147 cm^{-1} , it is centred at 2148 cm^{-1} in the first two spectra, but then it gradually moves to near 2144 cm^{-1} . Third, similarly, the band at 1532 cm^{-1} appears initially at 1536 cm^{-1} but then gradually moves to 1520 cm^{-1} . Fourth, the baseline is initially flat but then gradually begins to show a definite slope, indicating small particulate formation. These processes are associated with two molecules initially forming a complex. Then as the complex grows, proton transfer occurs, causing the disappearance of the band near 3510 cm^{-1} , slight shifts in the bands at 2148 and 1536 cm^{-1} , and a slope in the baseline. Such particulate formation in the gas-phase region and proton transfer has been observed for other ionic compounds, such as ammonium nitrate. In addition, Hammerl et al.¹⁷ also detected a band near 2147 cm^{-1} during slow decomposition of TAGzT; it was attributed to the formation of carbodiimide HNCNH .

Fig. 8 shows data obtained from ToFMS experiments. Peaks corresponding to products seen in the FTIR spectra are identified here. The peak at $m/z=26$ could either indicate CN radical formed during the decomposition process or a fragment

of HCN. The copious amount of N_2 ($m/z=28$) is produced due to the decomposition of the azotetrazolate ring. The strong peak at $m/z=32$ indicates the presence of hydrazine.

Since the intensity of hydrazine is large in the ToFMS data, it must also be present in the IR spectra. However, due to the overlapping of bands from NH_3 and HCN, the presence of hydrazine could not be detected easily. In order to confirm its presence, hydrazine obtained from Sigma Aldrich was vaporized at 140 °C and its FTIR spectrum acquired. The FTIR spectrum of hydrazine was plotted alongside the FTIR spectrum of the gas-phase decomposition products of TAGzT, as shown in Fig. 7. It is observed that hydrazine is present during the initial stages of decomposition. From Fig. 7, it is clear that hydrazine is present only during the initial phase of decomposition, and its formation rate decreases as the decomposition proceeds, as it is absent in the later spectra. Bands corresponding to heavier fragments are also observed.

The major question that arises from studying the FTIR spectrum is the identification of a strong peak at 2147 cm^{-1} . Tappan et al. suggested cyanamide as a major species of decomposition of TAGzT.¹⁸ The absorption bands corresponding to cyanamide are not present in our data. However, cyanamide is a very reactive species and is rapidly converted to its dimer N-cyanoguanidine, even at room temperature.

According to discussion of IR data by Socrates, it is known that in the region from 2000 to 2200 cm^{-1} , one of the following structures shows a distinct peak: $\text{N}\equiv\text{C}$, $\text{C}\equiv\text{N}$, $\text{N}\equiv\text{N}$, $\text{C}\equiv\text{C}$ and $\text{X}=\text{X}=\text{X}$ where X could be either N or C.⁴⁷ Using the information available from the mass spectra shown in Fig. 8, various compounds (based on m/z ratio) were studied having any of the above structures. Three classes of compounds were studied in order to identify the absorption band at 2147 cm^{-1} : azides, nitriles, and isonitriles. In general, azides exhibit a strong band around 2100 cm^{-1} corresponding to $\text{N}=\text{N}^+=\text{N}^-$ asymmetric stretch, whereas the symmetric stretch appears in the range

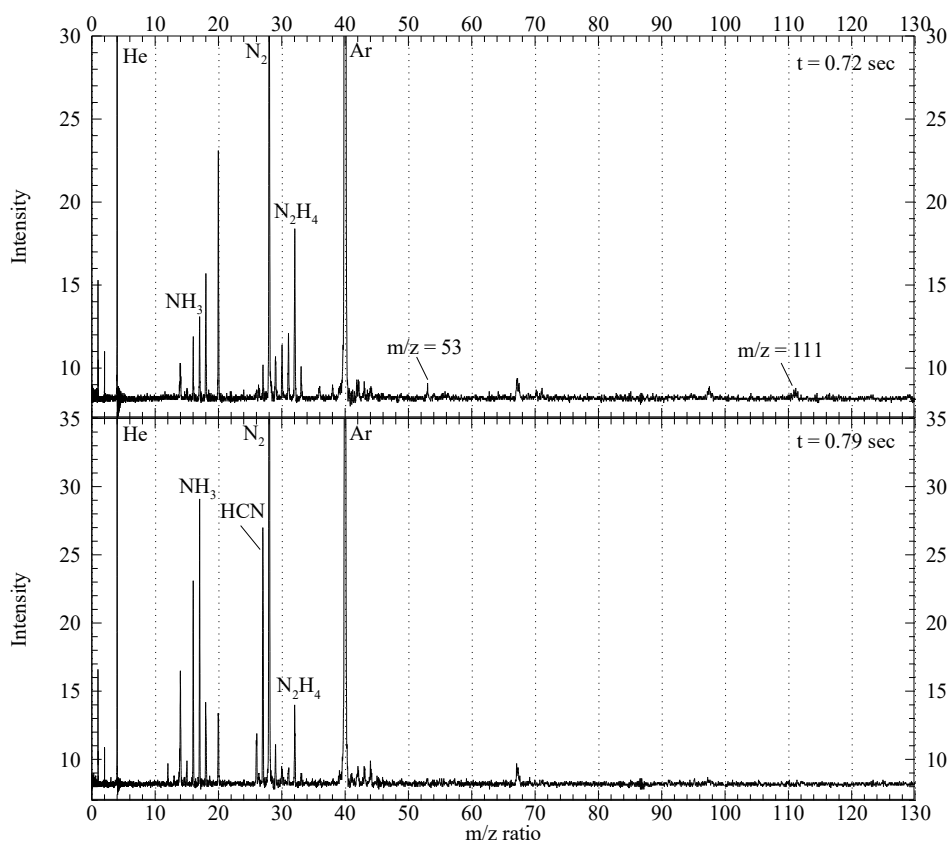


Fig. 8 Mass spectrum showing species evolved during the decomposition of TAGzT at 260 °C and 1 atm Ar & He.

1100-1300 cm^{-1} . However, in crystalline or complex form, the symmetric band may be of much weaker intensity. By comparing several nitriles and isonitriles, it was inferred that the stretching frequency for isonitrile was lower by approximately 100 cm^{-1} than a nitrile.⁴⁸ Based on the above information, the band at 2147 cm^{-1} could belong to either an azide or isocyanamide (NH_2NC). Isocyanamide is eliminated for several reasons. First, $\text{C}\equiv\text{N}$ stretching possesses a P and R branch character, as shown by cyanamide. This feature is absent in Fig. 7. Secondly, isocyanamide is unstable and should rearrange itself to form the more stable isomers cyanamide or carbodiimide, none of which were observed in the FTIR data. And third, the $\text{C}\equiv\text{N}$ stretching frequency for isocyanamide is 2159 cm^{-1} .⁴⁹ After studying several azides, nitriles and isonitriles along with our molecular modelling results the band at 2147 cm^{-1} is attributed to 3-azido-1H-1,2,4-triazole in the gas phase and 3-azido-1,2,4-triazol-4-ide anion in the condensed phase. The formation of these two molecules is explained in detail in the next section. This claim is further supported by the mass spectroscopy data shown in Fig. 8. The peak at $m/z=111$ is likely due to protonated 3-azido-1H-1,2,4-triazole.

Molecular modelling results

A chemical reaction mechanism for liquid-phase decomposition of TAGzT has been derived through quantum chemical calculations as described in molecular modelling section. The formation of its major decomposition products (N_2 , HCN, N_2H_4 , NH_3 , triaminoguanidine and the 3-azido-1,2,4-triazol-4-ide anion) is explained. Reactions in the mechanism presented here

were formulated by using our experimental results as a guide, and they include unimolecular decomposition, bimolecular and ion recombination, proton transfer, and isomeric rearrangement. It should be noted that a transition state for proton transfer within the liquid phase from the triaminoguanidinium cation to the azotetrazolate dianion as described by others^{17, 19, 50} for similar compounds could not be identified in our calculations. These ions prefer to stay separated in the liquid phase due to the solvation effect. Same has been reported for the ions in ammonium perchlorate by Zhu and Lin.⁵¹ Their calculation results suggest that a strong solvent effect exists on the dissociation kinetics in solution.

Quantum chemical calculations are helpful in deciding which reactions to exclude from the mechanism based on thermodynamic arguments. If a reaction is found to be highly endothermic, or considerably more endothermic than a competing pathway, then that reaction may be omitted from the mechanism in most cases. Transition state theory estimates of the rate constants can be used for making similar arguments. Thus, thermodynamic parameters and rate coefficient values were used to eliminate certain reactions from this mechanism. The computational approach adopted for developing the chemical reaction mechanism in this work is similar to that of Liu et al.²² Based on this methodology, the liquid-phase decomposition of TAGzT can be explained as follows.

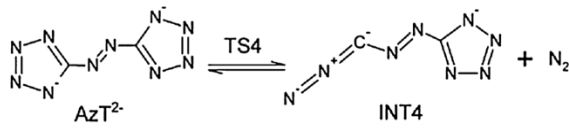
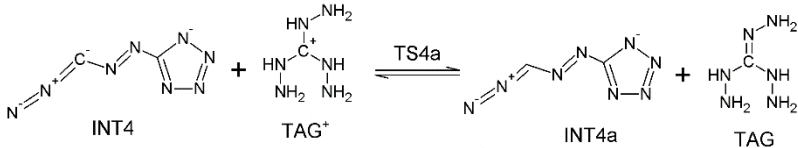
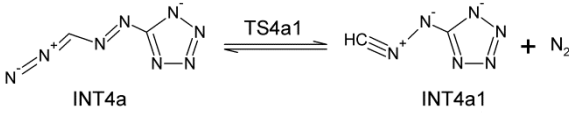
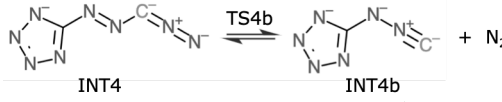
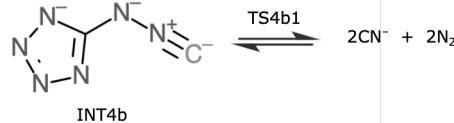
Formation of N_2 . Based on the quantum chemical calculations, important chemical reactions in the decomposition of TAGzT that result in the production of molecular nitrogen are listed in Table 1 with their corresponding thermodynamic parameters.

Gibbs free energies in the forward and reverse directions are provided and can be used for estimating the reaction rate constants using the thermodynamic formulation of the conventional transition state theory.⁵² In addition, enthalpy of reaction is provided to show the endothermic or exothermic nature of the reactions. Structures and coordinates of all the intermediate species and transition states are provided as supplementary information (ESI[†]). The mechanism of N₂ formation from AzT²⁻ during the decomposition of TAGzT is the same as that in the case of GzT.⁴⁴ It is included here for reference. Decomposition is initiated via the opening of one of the two five-membered rings in AzT²⁻ to release N₂ forming an ionic intermediate INT4 (reaction R1).⁴⁴ The carbon atom in INT4, which is no longer a part of the ring, acts as a nucleophile with the highest partial negative charge and easily accepts the proton from TAG⁺ resulting in the formation of INT4a and triaminoguanidine (reaction R2). Although a transition state structure was detected for R2, practically it has no energy barrier and is exothermic. INT4a then undergoes elimination of one more N₂ molecule to give INT4a1 (reaction R3). From INT4a1, the decomposition proceeds as described by Neeraj et al.⁴⁴ for GzT, but all the pathways that GzT follow do not exist in case of TAGzT. INT4 can also undergo successive unimolecular decomposition to release N₂ and CN⁻ (reactions R4 and R5). Apart from AzT²⁻, TAG which is formed in reaction R2 also acts as a source of N₂. TAG releases N₂ via a unimolecular decomposition pathway as shown in reactions R6 and R7. Reactions R2–R7 are characterized by lower Gibbs free energies

of activation in the forward direction than in the reverse direction making them the preferred pathways for N₂ formation. It should be noted that some reactions discussed in the later sections also contribute to the formation of N₂.

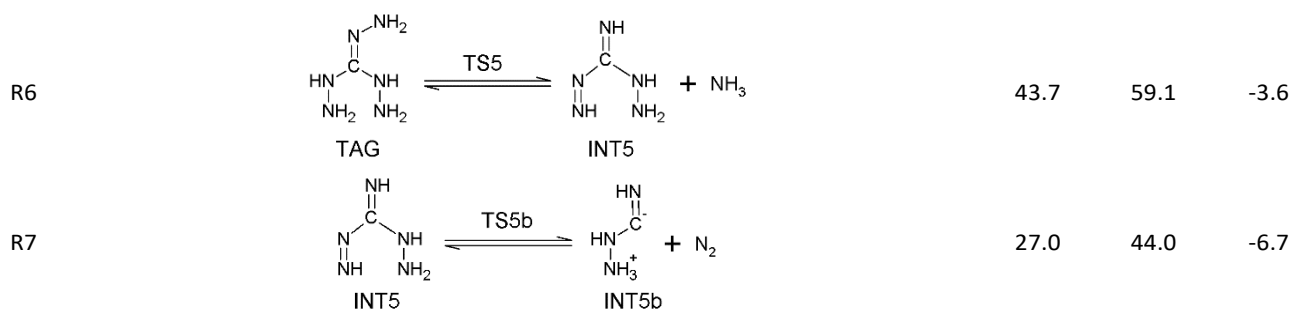
An alternate pathway possible for N₂ formation is proton transfer from TAG⁺ to AzT²⁻ followed by N₂ release. However, it is doubtful that proton transfer is important as an initiation mechanism for the following two reasons. First, if we assume that either one or both of the tetrazole rings are protonated, then the resulting ring-opening reactions releasing N₂ have forward free energy barriers of only 27 kcal/mol and 23.8 kcal/mol, respectively. With such low barriers, decomposition would occur at much lower temperatures than those needed in the thermolysis experiments. Second, if we compare with the activation energies proposed by Hammerl et al. of 39.1 kcal/mol, it is very close to the barrier suggested here of 37.5 kcal/mol (reaction R1).¹⁷ The agreement improves if we employ the relationship between an experimentally determined activation energy E_a and the computed enthalpic barrier given by $E_a = \Delta H^\ddagger + RT$, as described by Laidler.⁵³ The enthalpic barrier is nearly identical to the free energy barrier due to a unimolecular reaction; here, we use CBS-QB3 level of theory, for which $\Delta H^\ddagger = 38.4$ kcal/mol. By adding $RT \approx 1$ kcal/mol, we are within 0.3 kcal/mol of the experimentally determined activation energy. Hence, to the best of our understanding, N₂ elimination from singly or doubly protonated AzT²⁻ should not play a crucial role in the initiation of TAGzT decomposition.

Table 1 Reactions in the decomposition process of TAGzT resulting in the formation of N₂ along with thermodynamic parameters calculated at the CBS-QB3 level of theory.

No.	Reaction	$\Delta G_{r, f}^\ddagger$ ^a	$\Delta G_{r, r}^\ddagger$ ^b	ΔH_{rxn} ^c
R1		37.5	29.3	20.2
R2		-3.2	15.1	-18.5
R3		24.7	60.1	-24.9
R4		2.4	59.1	-46.7
R5		32.4	151.1	-86.6

PAPER

PCCP

^aGibbs free energy of activation in the forward direction (kcal/mol).^bGibbs free energy of activation in the reverse direction (kcal/mol).^cEnthalpy of reaction (kcal/mol).

Formation of HCN. Important chemical reactions in the decomposition of TAGzT that result in the production of HCN are listed in Table 2. Structures and coordinates of all the intermediate species and transition states are provided as supplementary information (ESI[†]). INT4a1 formed from reaction R3 can react with TAG⁺ via reaction R8. In this reaction, a proton from TAG⁺ transfers to the non-ring N atom of INT4a1. This proton transfer alters the C–N bond and destabilizes the ring, which opens, resulting in the formation of the cyanide anion (CN⁻), HCN, and N₂. An autocatalytic effect of TAG⁺ is observed in this reaction. Such autocatalysis may also occur for other

reactions discussed in this work. The cyanide anion formed from reactions R5 and R8 can readily abstract a hydrogen atom from TAG⁺ and HNC to form HCN, refer reaction R9 and R10. HNC formation is discussed later (reaction R14). It should be noted that reaction R8 in Table 2 is highly exothermic. Such high exothermicity is expected for these reactions because C≡N and N≡N bonds are formed. Formation of N₂ in this manner with the release of a high amount of energy is the process that makes high-nitrogen compounds such as TAGzT attractive as propellant ingredients.

Table 2 Important reactions in the decomposition of TAGzT resulting in the formation of HCN along with thermodynamic parameters calculated at the CBS-QB3 level of theory.^a

No.	Reaction	ΔG_f^\ddagger	ΔG_r^\ddagger	ΔH_{rxn}
R8		37.5	166.5	-97.1
R9		3.3	2.8	0.6
R10	HNC + CN ⁻ ⇌ HCN + CN ⁻	0.0 ^d	15.53	-14.64

^aSee footnote of Table 1 for various definitions.^dNo TS found. Assume barrierless reaction.

Formation of N₂H₄. N₂H₄ is observed early in the TAGzT decomposition process. Important reactions leading to the formation of N₂H₄ are listed in Table 3. Structures and coordinates of all the intermediate species and transition states are provided as supplementary information (ESI[†]). Due to proton transfer reactions R2 and R9, both TAG⁺ and TAG are present in the liquid phase. They may combine to form a positively charged intermediate INT1 (reaction R11). The forward free energy barrier for this reaction is low. In TAG, the most preferred site for bond formation is the imine nitrogen. Our calculations showed that a similar reaction involving a combination of two neutral TAG molecules has very high activation energy and hence is not considered here. Once INT1 is formed, it undergoes rearrangement as shown in reaction R12 which involves a hydrogen atom transfer to form INT1a. N₂H₄ is

formed in reaction R13 by unimolecular decomposition of INT1a. Reaction R14 shows an additional feasible pathway for N₂H₄ formation. It involves unimolecular decomposition of INT5 which is formed from reaction R6.

N₂H₄ is one of the major products of TAGzT decomposition and its rapid reactions with nitrogen oxides contribute to the observed burn rate enhancement when TAGzT is an ingredient in solid propellants.^{6, 7, 54} Since R13 is an important reaction in TAGzT decomposition and involves considerably large molecules, a comparison of various methods which were used in quantum chemical calculations is given in Table 4. It can be observed that with the exception of the results from the use of the B3LYP/6-311++G(d,p) level of theory, there appears to be only a relatively small variation in the thermodynamic parameters calculated using various levels of theory.

Table 3 Important reactions in the decomposition of TAGzT resulting in the formation of N₂H₄ along with thermodynamic parameters calculated at the CBS-QB3 level of theory.^a

No.	Reaction	ΔG_f^\ddagger	ΔG_r^\ddagger	ΔH_{rxn}
R11		31.2	13.6	3.1
R12		5.9	1.2	4.0
R13		12.2	17.9	8.6
R14		30.7	85.0	-33.0

^aSee footnote of Table 1 for various definitions.

Table 4 Thermodynamic parameters for reaction R13 calculated using various levels of theory.

Reaction R13: INT1a ⇌ INT1a1 + N ₂ H ₄						
Theory and basis set	ΔH_f^\ddagger ^a	ΔH_r^\ddagger ^b	ΔH_{rxn} ^c	ΔG_f^\ddagger ^d	ΔG_r^\ddagger ^e	ΔG_{rxn} ^f
B3LYP/6-311++G(d,p) ³²	5.84	12.7	-6.9	4.8	25.9	-21.1
CBS-QB3 ³⁵	12.9	4.3	8.6	12.2	17.9	-5.7
MP2/6-311++G(d,p) ³⁶	14.9	2.1	12.8	13.3	14.9	-1.5
M062X/6-311++G(d,p) ⁵⁵	11.0	2.6	8.3	10.1	15.9	-5.8
G4(MP2) ³⁷	13.5	4.8	8.7	12.6	18.0	-5.4

^aActivation enthalpy in the forward direction (kcal/mol).

^bActivation enthalpy in the reverse direction (kcal/mol).

^cEnthalpy of reaction (kcal/mol).

^dGibbs free energy of activation in the forward direction (kcal/mol).

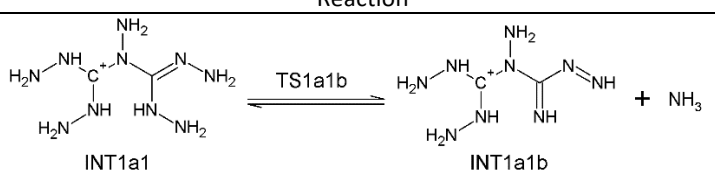
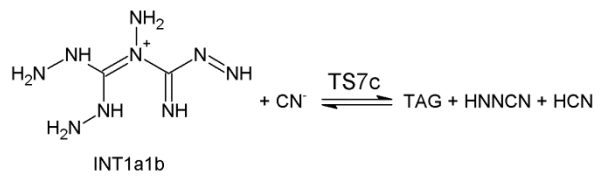
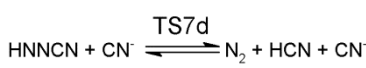
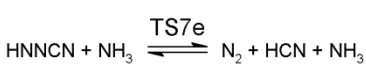
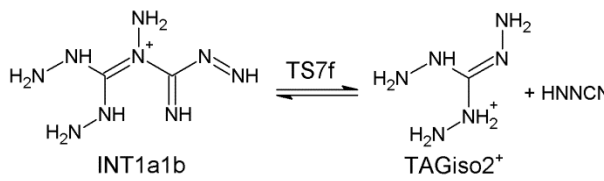
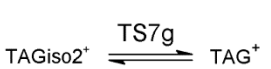
^eGibbs free energy of activation in the reverse direction (kcal/mol).

^fGibbs free energy of reaction (kcal/mol).

Formation of NH₃. In our CRT experiments, we observed that N₂H₄ and NH₃ evolve in the initial stages of TAGzT decomposition. This indicates that similar to N₂H₄, NH₃ is also formed from TAG. Important pathways for NH₃ formation are shown in Table 5. Structures and coordinates of all the intermediate species and transition states are provided as supplementary information (ESI[†]). INT1a1 formed from reaction R13 undergoes intramolecular H atom transfer followed by its unimolecular decomposition in reaction R15. The reverse barrier for this reaction is significantly higher than the forward barrier. Moreover, NH₃ molecules readily escape the sample during thermolysis and do not accumulate in any significant amount. Hence the reverse reaction R15 is not important. INT1a1b regenerates TAG and TAG⁺ via a unimolecular and a

bimolecular pathway, respectively (reactions R16, R19, and R20). HNNCN is also produced from both the pathways. HNNCN reacts with CN⁻ or NH₃ to form N₂ and HCN (reactions R17 and R18). NH₃ can also be formed by a series of molecular rearrangements of TAG molecule followed by unimolecular decomposition reactions. Our calculations showed that these reactions have relatively high free energy barriers in the forward direction and hence are not included here.

Table 5 Important reactions in the decomposition of TAGzT resulting in the formation of NH₃ along with thermodynamic parameters calculated at the CBS-QB3 level of theory.^a

No.	Reaction	ΔG_f^\ddagger	ΔG_r^\ddagger	ΔH_{rxn}
R15		36.8	46.9	1.7
R16		5.3	14.7	1.2
R17		4.5	79.5	-69.1
R18		12.4	87.4	-69.1
R19		34.2	19.3	28.2
R20		24.5	51.5	-26.9

^aSee footnote of Table 1 for various definitions.

Formation of 3-azido-1,2,4-triazol-4-ide anion. During the decomposition of GzT, once the anion INT4a1 is formed it can react with guanidinium cation (Gu^+) in numerous ways giving rise to multiple parallel pathways.⁴⁴ All the analogous transition states for reactions between INT4a1 and TAG^+ for TAGzT could not be obtained. Instead, in the case of TAGzT, INT4a1 undergoes the reactions shown in Table 6. Structures and coordinates of all the intermediate species and transition states are provided as supplementary information (ESI[†]). The terminal C atom in INT4a1 bonds with one of the ring N atoms thereby closing the ring to form the negatively charged intermediate INT4a1b as shown in reaction R21. This is followed by breaking of the N–N bond in the tetrazole ring leading to the formation of 3-azido-1,2,4-triazol-4-ide anion via reaction R22. INT4b, formed from reaction R4, can also undergo reactions similar to R21 and R22 but our calculations showed that those reactions have relatively low free energy barriers in the reverse direction and hence are not included here. Reactions R23–R25 show that the azide anion decomposes quite readily and each reaction is exothermic. In the presence of a proton donating species, such as HCN, the azide anion readily converts to 3-azido-1H-1,2,4-triazole (reaction R26). N₂ release from 3-azido-1H-1,2,4-triazole is shown in reaction R27. Frequency calculations for the optimized structures of 3-azido-1,2,4-triazol-4-ide anion and 3-

azido-1H-1,2,4-triazole were performed with B3LYP functional and results are provided in Table S2 of the supplementary material (ESI[†]). Biczysko et al. showed that fundamental frequencies can be calculated with remarkable accuracy at B2PLYP/N07D and B2PLYP/aug-cc-pVTZ levels of theory.^{56–59} Hence, frequency calculations were also performed at these relatively more computationally expensive levels of theory. Anharmonic corrections were applied to obtain accurate frequency data. At B2PLYP/N07D level of theory, the calculated frequencies of $\text{N}=\text{N}^+=\text{N}^-$ asymmetric stretch in 3-azido-1,2,4-triazol-4-ide anion and 3-azido-1H-1,2,4-triazole were 2134 cm^{-1} and 2153 cm^{-1} , respectively. Anharmonic calculations did not converge at B2PLYP/aug-cc-pVTZ level. At B2PLYP/aug-cc-pVTZ level of theory, the calculated harmonic frequencies of $\text{N}=\text{N}^+=\text{N}^-$ asymmetric stretch in 3-azido-1,2,4-triazol-4-ide anion and 3-azido-1H-1,2,4-triazole were 2164 cm^{-1} and 2183 cm^{-1} , respectively. After accounting for the margin of error in calculations and experiment this is in suitable agreement with the value, 2147 cm^{-1} observed in our FTIR tests for TAGzT (shown in Fig. 6 and Fig. 7). For GzT the band at 2147 cm^{-1} is very weak for condensed phase decomposition residue and is not even observed in the gas-phase decomposition species.⁴⁴ This indicates that reactions R21 and R22 are not likely to be important in the decomposition of GzT.

Table 6 Important reactions in the decomposition of TAGzT resulting in the formation of 3-azido-1,2,4-triazol-4-ide anion along with thermodynamic parameters calculated at the CBS-QB3 level of theory.^a

No.	Reaction	ΔG_f^\ddagger	ΔG_r^\ddagger	ΔH_{rxn}
R21	 INT4a1 $\xrightleftharpoons{TS4a1b}$ INT4a1b	14.0	46.3	-34.4
R22	 INT4a1b $\xrightleftharpoons{TS4a1b1}$ 3-azido-1,2,4-triazol-4-ide	20.8	26.2	-3.5
R23	 3-azido-1,2,4-triazol-4-ide $\xrightleftharpoons{TS4a1b2}$ 1,2,4-triazol-4-ide anion + N ₂	31.3	46.3	-4.2
R24	 1,2,4-triazol-4-ide anion $\xrightleftharpoons{TS4a1b3}$ HC ⁻ -N≡N + N ₂	9.5	41.1	-19.6
R25	 HC ⁻ -N≡N $\xrightleftharpoons{TS4a1b4}$ HCN + CN ⁻	25.1	67.8	-36.3
R26	 1,2,4-triazol-4-ide anion + HCN $\xrightleftharpoons{TS4a1b5}$ 3-azido-1H-1,2,4-triazole + CN ⁻	5.3	5.6	-0.3
R27	 3-azido-1H-1,2,4-triazole $\xrightleftharpoons{TS4a1b6}$ 1,2,4-triazol-4-ide anion + N ₂	34.4	31.6	14.0

^aSee footnote of Table 1 for various definitions.

Conclusions

Liquid-phase decomposition of TAGzT was studied using FTIR spectroscopy and time-of-flight mass spectroscopy. The formation of different chemical species observed in these studies was explained using quantum chemical calculations. Major reaction pathways were identified based on thermodynamic considerations. Within the framework of experiments and calculations in the present work, the following conclusions can be drawn.

1. When subjected to thermolysis, TAGzT decomposes rapidly at temperatures above 230 °C in the liquid phase and the major decomposition products are N₂, N₂H₄, NH₃, HCN and 3-azido-1,2,4-triazol-4-ide anion.
2. TAGzT decomposition is initiated within AzT²⁻ dianion as evident from the early disappearance of the characteristic bands of AzT²⁻.
3. Proton transfer takes place only after ring opening has occurred and it is a very rapid, barrier-less reaction.
4. The energetic material characteristics of TAGzT are a result of the HCN and N₂ producing reactions which are revealed by molecular modelling calculations to be highly exothermic.

5. CRT tests show that decomposition of TAGzT is more rapid as compared GzT. This is confirmed from the values of thermodynamic parameters calculated for reactions involved in the decomposition mechanism of these compounds.

Conflicts of interest

There are no conflicts to declare.

Acknowledgements

The authors acknowledge the support from the Air Force Office of Scientific Research under grant number FA9550-13-1-0004. Also, this material is based upon work supported by, or in part by, the U. S. Army Research Laboratory and the U. S. Army Research Office under grant numbers W911NF-08-1-0124 and W911NF-15-1-0202. The authors are grateful to Dr. D. E. Chavez of Los Alamos National Laboratory for providing the sample of TAGzT used in this work.

References

1. R. P. Singh, H. Gao, D. T. Meshri and J. M. Shreeve, ed. T. M. Klapötke, Springer, Berlin, Heidelberg, 2007, **125**, 35-83. DOI: 10.1007/430_2006_055.
2. M. A. Hiskey, N. Goldman and J. R. Stine, *Journal of Energetic Materials*, 1998, **16**, 119-127. DOI: 10.1080/07370659808217508.
3. D. E. Chavez and M. A. Hiskey, *Journal of Energetic Materials*, 1999, **17**, 357-377. DOI: 10.1080/07370659908201796.
4. N. Wingborg and N. V. Latypov, *Propellants, Explosives, Pyrotechnics*, 2003, **28**, 314-318. DOI: 10.1002/prop.200300022.
5. C. Walsh and C. Knott, JANNAF *Propellant Development and Compatibility Subcommittee Meeting, Charlottesville, Virginia*, 2003.
6. B. A. Mason, J. M. Lloyd, S. F. Son and B. C. Tappan, *International Journal of Energetic Materials and Chemical Propulsion*, 2009, **8**, 31-38. DOI: 10.1615/IntJEnergeticMaterialsChemProp.v8.i1.30.
7. N. Kumbhakarna, S. T. Thynell, A. Chowdhury and P. Lin, *Combustion Theory and Modelling*, 2011, **15**, 933-956. DOI: 10.1080/13647830.2011.591503.
8. R. Behrens, D. Wiese-Smith and H. F. Hayden, 41st JANNAF Combustion Subcommittee Meeting, San Diego, CA, 2006.
9. M. Szala, M. Hara, L. Szymańczyk and Z. Surma, *Propellants, Explosives, Pyrotechnics*, 2017, **42**, 1278-1282. DOI: 10.1002/prop.201700090.
10. T. B. Brill and P. J. Brush, *Philosophical Transactions of the Royal Society of London. Series A: Physical and Engineering Sciences*, 1992, **339**, 377-385. DOI:10.1098/rsta.1992.0043
11. R. A. Yetter, F. L. Dryer, M. T. Allen and J. L. Gatto, *Journal of Propulsion and Power*, 1995, **11**, 683-697. DOI: 10.2514/3.23894.
12. D. Chakraborty, R. P. Muller, S. Dasgupta and W. A. Goddard, *Journal of Computer-Aided Materials Design*, 2001, **8**, 203-212. DOI: 10.1023/A:1020074113000.
13. L. Patidar and S. T. Thynell, *Combustion and Flame*, 2017, **178**, 7-20. DOI: 10.1016/j.combustflame.2016.12.024
14. L. Patidar, M. Khichar and S. T. Thynell, *Combustion and Flame*, 2018, **188**, 170-179. DOI: 10.1016/j.combustflame.2017.09.042.
15. A. J. Bracuti and R. Marchak, *Structural features of bis (triaminoguanidinium) bis (azotetrazolate)*, Army Armament Research Development and Engineering Center Picatinny Arsenal NJ Technical Research Center, 2005.
16. K. D. Behler, J. A. Ciezak-Jenkins and R. C. Sausa, *The Journal of Physical Chemistry A*, 2013, **117**, 1737-1743. DOI: 10.1021/jp311463g.
17. A. Hammerl, M. A. Hiskey, G. Holl, T. M. Klapötke, K. Polborn, J. Stierstorfer and J. J. Weigand, *Chemistry of Materials*, 2005, **17**, 3784-3793. DOI: 10.1021/cm050684f.
18. B. C. Tappan, A. N. Ali, S. F. Son and T. B. Brill, *Propellants, Explosives, Pyrotechnics*, 2006, **31**, 163-168. DOI: 10.1002/prop.200600023.
19. R. S. Damse, M. Ghosh, N. H. Naik and A. K. Sikder, *Journal of Propulsion and Power*, 2009, **25**, 249-256. DOI: 10.2514/1.35789.
20. H. F. Hayden, PhD thesis, The George Washington University, 2009.
21. N. Kumbhakarna and S. T. Thynell, *Thermochimica Acta*, 2014, DOI: 10.1016/j.tca.2014.02.014.
22. W. G. Liu, S. Wang, S. Dasgupta, S. T. Thynell, W. A. Goddard, S. Zybin and R. A. Yetter, *Combustion and Flame*, 2013, **160**, 970-981. DOI: 10.1016/j.combustflame.2013.01.012.
23. B. Yuan and E. R. Bernstein, *The Journal of Chemical Physics*, 2016, **144**, 234302. DOI: 10.1063/1.4953552.
24. B. Yuan and E. R. Bernstein, *The Journal of Chemical Physics*, 2016, **145**, 064306. DOI: 10.1063/1.4960345.
25. M. Khichar, L. Patidar and S. T. Thynell, *Combustion and Flame*, 2018, **198**, 455-465. DOI: 10.1016/j.combustflame.2018.10.005.
26. L. Patidar, M. Khichar and S. T. Thynell, *Combustion and Flame*, 2020, **212**, 67-78. DOI: 10.1016/j.combustflame.2019.10.025.
27. E. S. Kim, H. S. Lee, C. F. Mallery and S. T. Thynell, *Combustion and Flame*, 1997, **110**, 239-255. DOI: 10.1016/S0010-2180(97)00062-X.
28. C. F. Mallery and S. T. Thynell, *Combustion Science and Technology*, 1997, **122**, 113-129. DOI: 10.1080/00102209708935607.
29. A. Chowdhury and S. T. Thynell, *Thermochimica Acta*, 2006, **443**, 159-172. DOI: 10.1016/j.tca.2006.01.006.
30. M. R. Weismiller, S. Q. Wang, A. Chowdhury, S. T. Thynell and R. A. Yetter, *Thermochimica Acta*, 2013, **551**, 110-117. DOI: 10.1016/j.tca.2012.10.008.
31. M. J. Frisch, G. W. Trucks, H. B. Schlegel, G. E. Scuseria, M. A. Robb, J. R. Cheeseman, G. Scalmani, V. Barone, B. Mennucci, G. A. Petersson, H. Nakatsuji, M. Caricato, X. Li, H. P. Hratchian, A. F. Izmaylov, J. Bloino, G. Zheng, J. L. Sonnenberg, M. Hada, M. Ehara, K. Toyota, R. Fukuda, J. Hasegawa, M. Ishida, T. Nakajima, Y. Honda, O. Kitao, H. Nakai, T. Vreven, J. A. Montgomery, Jr., J. E. Peralta, F. Ogliaro, M. Bearpark, J. J. Heyd, E. Brothers, K. N. Kudin, V. N. Staroverov, T. Keith, R. Kobayashi, J. Normand, K. Raghavachari, A. Rendell, J. C. Burant, S. S. Iyengar, J. Tomasi, M. Cossi, N. Rega, J. M. Millam, M. Klene, J. E. Knox, J. B. Cross, V. Bakken, C. Adamo, J. Jaramillo, R. Gomperts, R. E. Stratmann, O. Yazyev, A. J. Austin, R. Cammi, C. Pomelli, J. W. Ochterski, R. L. Martin, K. Morokuma, V. G. Zakrzewski, G. A. Voth, P. Salvador, J. J. Dannenberg, S. Dapprich, A. D. Daniels, O. Farkas, J. B. Foresman, J. V. Ortiz, J. Cioslowski, and D. J. Fox, Gaussian 09, Revision D.01, Gaussian, Inc., Wallingford CT, 2013.
32. P. J. Stephens, F. J. Devlin, C. F. Chabalowski and M. J. Frisch, *The Journal of Physical Chemistry*, 1994, **98**, 11623-11627. DOI: 10.1021/j100096a001.
33. W. J. Hehre, R. Ditchfield and J. A. Pople, *The Journal of Chemical Physics*, 1972, **56**, 2257-2261. DOI: 10.1063/1.1677527.
34. R. Krishnan, J. S. Binkley, R. Seeger and J. A. Pople, *The Journal of Chemical Physics*, 1980, **72**, 650-654. DOI: 10.1063/1.438955.
35. J. A. Montgomery, M. J. Frisch, J. W. Ochterski and G. A. Petersson, *The Journal of Chemical Physics*, 1999, **110**, 2822-2827. DOI: 10.1063/1.477924.
36. M. Head-Gordon, J. A. Pople and M. J. Frisch, *Chemical Physics Letters*, 1988, **153**, 503-506. DOI: 10.1016/0009-2614(88)85250-3.
37. L. A. Curtiss, P. C. Redfern and K. Raghavachari, *The Journal of Chemical Physics*, 2007, **127**, 124105. DOI: 10.1063/1.2770701.
38. K. Fukui, *Accounts of Chemical Research*, 1981, **14**, 363-368. DOI: 10.1021/ar00072a001.
39. H. P. Hratchian and H. B. Schlegel, *The Journal of Chemical Physics*, 2004, **120**, 9918-9924. DOI: 10.1063/1.1724823.
40. J. Tomasi, B. Mennucci and E. Cancès, *Journal of Molecular Structure: THEOCHEM*, 1999, **464**, 211-226. DOI: 10.1016/S0166-1280(98)00553-3.
41. C. J. Cramer and D. G. Truhlar, *Chemical Reviews*, 1999, **99**, 2161-2200. DOI: 10.1021/cr960149m.
42. A. Fernández-Ramos, J. A. Miller, S. J. Klippenstein and D. G. Truhlar, *Chemical Reviews*, 2006, **106**, 4518-4584. DOI: 10.1021/cr050205w.
43. K. Yang, Y. H. Park, S. G. Cho, H. W. Lee, C. K. Kim and H.-J. Koo, *Journal of Computational Chemistry*, 2010, **31**, 2483-2492. DOI: 10.1002/jcc.21542.
44. N. R. Kumbhakarna, K. J. Shah, A. Chowdhury and S. T. Thynell, *Thermochimica Acta*, 2014, **590**, 51-65. DOI: 10.1016/j.tca.2014.06.005.

45. F. Billes, H. Endrédi and G. Keresztury, *Journal of Molecular Structure: THEOCHEM*, 2000, **530**, 183-200. DOI: 10.1016/S0166-1280(00)00340-7.
46. J. Stierstorfer, T. M. Klapötke, A. Hammerl and R. D. Chapman, *Zeitschrift für anorganische und allgemeine Chemie*, 2008, **634**, 1051-1057. DOI: 10.1002/zaac.200800003.
47. G. Socrates, *Infrared and Raman Characteristic Group Frequencies: Tables and Charts, 3rd edition*, Wiley, Chichester, 2001.
48. R. G. Gillis and J. L. Occolowitz, *Spectrochimica Acta*, 1963, **19**, 873-876. DOI: 10.1016/0371-1951(63)80174-5.
49. K. Ichikawa, Y. Hamada, Y. Sugawara, M. Tsuboi, S. Kato and K. Morokuma, *Chemical Physics*, 1982, **72**, 301-312. DOI: 10.1016/0301-0104(82)85127-6.
50. T. An, F.-Q. Zhao, Q. Wang, D.-L. Sheng, Q. Pan, H. Feng, J.-H. Yi and Y.-L. Wang, *Journal of Analytical and Applied Pyrolysis*, 2013, **104**, 405-411. DOI: 10.1016/j.jaap.2013.06.005.
51. R. S. Zhu and M. C. Lin, *Chemical Physics Letters*, 2006, **431**, 272-277. DOI: 10.1016/j.cplett.2006.10.007.
52. H. Eyring, *The Journal of Chemical Physics*, 1935, **3**, 107-115. DOI: 10.1063/1.1749604.
53. K. J. Laidler, *Chemical Kinetics*, Harper & Row, New York, 3 edn., 1987.
54. H. E. Perlee, A. C. Imhof and M. G. Zabetakis, *Journal of Chemical & Engineering Data*, 1962, **7**, 377-379. DOI: 10.1021/je60014a016.
55. Y. Zhao and D. G. Truhlar, *Theoretical Chemistry Accounts*, 2008, **120**, 215-241. DOI: 10.1007/s00214-007-0310-x.
56. S. Grimme, *The Journal of Chemical Physics*, 2006, **124**, 034108. DOI: 10.1063/1.2148954.
57. V. Barone, P. Cimino and E. Stendardo, *Journal of Chemical Theory and Computation*, 2008, **4**, 751-764. DOI: 10.1021/ct800034c.
58. M. Biczysko, P. Panek, G. Scalmani, J. Bloino and V. Barone, *Journal of Chemical Theory and Computation*, 2010, **6**, 2115-2125. DOI: 10.1021/ct100212p.
59. R. A. Kendall, T. H. Dunning and R. J. Harrison, *The Journal of Chemical Physics*, 1992, **96**, 6796-6806. DOI: 10.1063/1.462569.